IOP Publishing — Journal of Physics D: Applied Physics

J. Phys. D: Appl. Phys. **43** (2010) 073001 (13pp) doi:10.1088/0022-3727/43/7/073001

TOPICAL REVIEW

Properties of the state of the art of bulk III–V nitride substrates and homoepitaxial layers

Jaime A Freitas Jr

Naval Research Laboratory, Electronic Science and Technology Division–Electronic Materials Branch, Washington, DC 20375-5347, USA

E-mail: jaime.freitas@nrl.navy.mil

Received 2 December 2008
Published 3 February 2010
Online at stacks.iop.org/JPhysD/43/073001

Abstract

The technological importance of III–V nitride semiconductors relies on their variety of applications, which cover optical, optoelectronic and electronic devices capable of operating under extreme values of current, voltage and temperature. The major roadblock for full realization of the potential of nitride semiconductors is still the availability of affordable large-area and high-quality native substrates with controlled electrical properties. Despite the impressive accomplishments recently achieved by techniques such as hydride vapour phase epitaxy and ammonothermal for GaN and sublimation for AlN, much more must be attained before establishing a bulk growth technique of choice to grow these materials. A brief review of the structural, optical and electronic properties of the state of the art of bulk and thick-film (quasi-bulk) nitride substrates and homoepitaxial films is presented, and a few device applications are also highlighted.

(Some figures in this article are in colour only in the electronic version)

1. Introduction

The III–V nitride semiconductor material system possesses a unique combination of extreme values of fundamental physical and chemical parameters. This unusual characteristic places it as one of the most promising material systems for the fabrication of a variety of optoelectronic and electronic devices capable of performing under extreme conditions of power, frequency, temperature, and in harsh environments. The direct gap of AlN, GaN and InN, and its ternary and quaternary alloys covers the energy spectral range from 6.0 eV (∼207 nm) to 0.7 eV (∼1.77 μm). In addition, the wide bandgap of the nitride material system results in a low intrinsic carrier density that leads to low leakage and low dark current, a crucial property for photodetectors and high-temperature electronic applications. Despite the large carrier effective masses, leading to lower carrier mobilities, their high saturated velocity and high breakdown field make them adequate for high-frequency electronic device applications.

Presently, the major hurdle for full realization of the device potential based on the III–V nitrides material system is the lack of large-area, high crystalline quality native substrates with controlled electrical properties. Considerable progress has been accomplished lately on the growth of bulk AlN. Sublimation–recondensation (S–R) and physical vapour transport (PVT) have been successfully used to grow AlN boules with diameter between 10 and 50 mm. Unlike AlN, GaN does not sublime, precluding the use of these techniques for bulk GaN growth. High-pressure and low-pressure solution growth techniques, ammonothermal (a modification of the successful hydrothermal technique used to grow quartz) and other implemented approaches have been employed to address the technical difficulties of bulk GaN growth. This lack of adequate substrates for homoepitaxial growth compelled the material scientist to develop a deep understanding of the nucleation process and to optimize the properties of nucleation (buffer) layers necessary to mitigate problems related to heteroepitaxial growth [1, 2]. As a result, the

 © 2010 IOP Publishing Ltd Printed in the UK

Report Documentation Page

Form Approved
OMB No. 0704-0188

Public reporting burden for the collection of information is estimated to average 1 hour per response, including the time for reviewing instructions, searching existing data sources, gathering and maintaining the data needed, and completing and reviewing the collection of information. Send comments regarding this burden estimate or any other aspect of this collection of information, including suggestions for reducing this burden, to Washington Headquarters Services, Directorate for Information Operations and Reports, 1215 Jefferson Davis Highway, Suite 1204, Arlington VA 22202-4302. Respondents should be aware that notwithstanding any other provision of law, no person shall be subject to a penalty for failing to comply with a collection of information if it does not display a currently valid OMB control number.

1. REPORT DATE	2. REPORT TYPE	3. DATES COVERED
DEC 2008		**00-00-2008 to 00-00-2008**

4. TITLE AND SUBTITLE
Properties of the state of the art of bulk III-V nitride substrates and homoepitaxial layers

5a. CONTRACT NUMBER
5b. GRANT NUMBER
5c. PROGRAM ELEMENT NUMBER

6. AUTHOR(S)

5d. PROJECT NUMBER
5e. TASK NUMBER
5f. WORK UNIT NUMBER

7. PERFORMING ORGANIZATION NAME(S) AND ADDRESS(ES)
Naval Research Laboratory,4555 Overlook Avenue SW,Washington,DC,20375

8. PERFORMING ORGANIZATION REPORT NUMBER

9. SPONSORING/MONITORING AGENCY NAME(S) AND ADDRESS(ES)

10. SPONSOR/MONITOR'S ACRONYM(S)

11. SPONSOR/MONITOR'S REPORT NUMBER(S)

12. DISTRIBUTION/AVAILABILITY STATEMENT
Approved for public release; distribution unlimited

13. SUPPLEMENTARY NOTES

14. ABSTRACT
The technological importance of III?V nitride semiconductors relies on their variety of applications, which cover optical, optoelectronic and electronic devices capable of operating under extreme values of current, voltage and temperature. The major roadblock for full realization of the potential of nitride semiconductors is still the availability of affordable large-area and high-quality native substrates with controlled electrical properties. Despite the impressive accomplishments recently achieved by techniques such as hydride vapour phase epitaxy and ammonothermal for GaN and sublimation for AlN, much more must be attained before establishing a bulk growth technique of choice to grow these materials. A brief review of the structural, optical and electronic properties of the state of the art of bulk and thick-film (quasi-bulk) nitride substrates and homoepitaxial films is presented, and a few device applications are also highlighted.

15. SUBJECT TERMS

16. SECURITY CLASSIFICATION OF:			17. LIMITATION OF ABSTRACT	18. NUMBER OF PAGES	19a. NAME OF RESPONSIBLE PERSON
a. REPORT	b. ABSTRACT	c. THIS PAGE			
unclassified	**unclassified**	**unclassified**	**Same as Report (SAR)**	**13**	

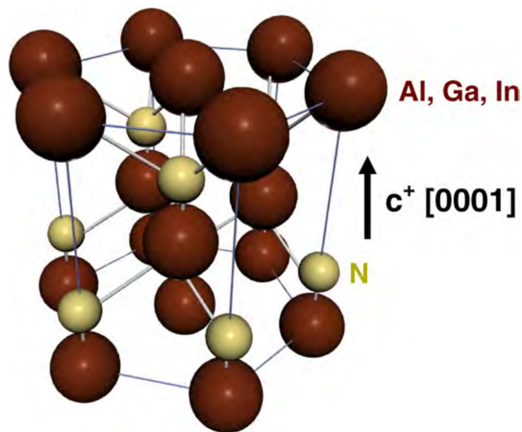

Figure 1. Schematic diagram of III/V nitrides wurtzite structure. The sequence of the group III and nitrogen in the bilayer determines the crystal polarity.

Figure 2. Picture of a 2 inch AlN on-axis (c-axis) wafer with ∼85% usable area. The wafer was cut from a single crystal boule. (Courtesy of L Schowalter, CIS, USA.)

deposition of device-quality films on foreign substrates such as sapphire, Si and SiC, among others, was accomplished. These heteroepitaxial films are characterized by reduced intrinsic n-type background carrier concentration, which allows carrier type control, and relatively smooth surface and improved crystalline quality [3]. Such templates have been successfully employed to fabricate a number of commercial optoelectronic and electronic devices [4, 5].

Despite these remarkable achievements, the properties of thin heteroepitaxial nitride films are still seriously limiting the performance of devices demanding higher material yields, e.g. solid state lighting (SSL, which requires high quantum efficiency LED), laser diodes (LD) and high-frequency/high-power electronic devices (e.g. FETS, HEMTs). The high growth temperature usually required to produce these wide bandgap materials exacerbates fundamental material problems such as residual stress, difference in thermal expansion coefficient, low energy defect formation and impurity incorporation. In addition, doping activation and self-compensation are difficult to control at the typically high deposition temperatures. Furthermore, the high concentration of dislocations, resulting mostly from lattice constant mismatch, typically on the order of 10^9–10^{11} cm^{-2}, must be reduced to improve device performance. Overcoming these limitations will require the use of native substrates to grow electronic grade homoepitaxial layers.

The commonly used techniques to grow bulk AlN and GaN, and a few new approaches are briefly discussed. Also, a concise discussion of the structural, optical and electronic properties of bulk and epitaxial films of AlN and GaN is presented. In addition, a few examples of optical and electronic devices fabricated on bulk substrates are highlighted.

2. Growth of III-nitride substrates

The III–V nitride (III–V/N) semiconductors crystallize in the wurtzite structure and cubic structures, such as zinc blende (sphalerite) or rock salt. The thermodynamically stable grown structures are wurtzite for bulk AlN, GaN and InN (figure 1) and zinc blende for BN. The rock salt structure is stable only at elevated pressures [6–8]. The cubic (zinc blende) phase of GaN and InN are metastable and have been realized only in thin heteroepitaxial films deposited on highly mismatched substrates (0 0 1) oriented substrates, e.g. GaAs, InAs, MgO, Si and β-SiC [9–14].

Bulk III–V/N cannot be grown from the stoichiometric melts by well-established techniques such as Czochralski or Bridgman because of the extremely high melting temperatures and very high nitrogen decomposition pressures [15–17]. Therefore, crystal growers across the world have modified or adapted different methods requiring lower temperatures and pressures to grow bulk AlN and GaN semiconductors.

2.1. Growth of bulk and thick-film AlN

S–R, vaporization (PVT) and solution routes have been successfully used to grow bulk AlN crystals [18]. The nitrogen vapour pressure over AlN is six orders of magnitude lower than over GaN, which makes it possible to grow bulk crystals at atmospheric or sub-atmospheric pressure [19]. Due to the excessively high melting point, estimated over 2800 °C, AlN cannot be grown from the melt. Bulk AlN has been successfully grown by sublimation, but the high reactivity of aluminium gas at high sublimation temperatures (typically around 2000 °C) raises problems with regard to AlN purity and crucible stability [20–22]. The largest S–R crystal dimension previously reported was 470 mm^3 [22, 23]. The AlN precursor for this technique, prepared by direct reaction of aluminium powder and nitrogen at 1850 °C, was sealed in a tungsten crucible and an unseeded multi-grain crystal grew at the rate of 0.3 mm h^{-1} at 2250 °C in a nitrogen atmosphere. Boules grown by the S–R technique, with growth rate of about 1 mm h^{-1}, have improved considerably, and wafers of 2 inch diameter with a usable area of about 85% are produced (figure 2). These wafers contain large domains, which typically show x-ray diffraction (XRD) rocking curves with full width at half maximum (FWHM) of around 28 arcsec and 32 arcsec for symmetric and asymmetric, respectively, and dislocation density less than 10^4 cm^{-2} [24–27].

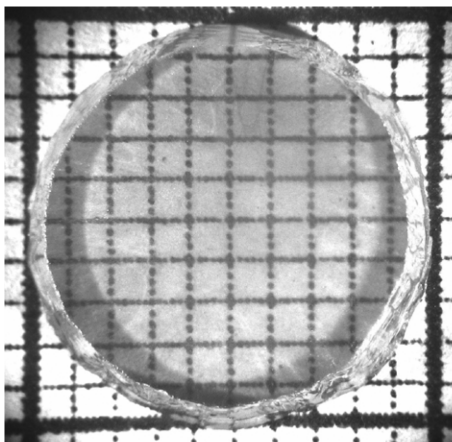

Figure 3. Photograph of a 3 mm thick and 10 mm diameter crack-free AlN boule grown by PVT. (Courtesy of Z Sitar, DMS&E, NCSU, USA.)

Bulk growth techniques that minimize the effects associated with container reactions and impurity inclusions are highly desirable. Bulk AlN crystals with centimetre-sized areas have been fabricated using RF energy, oscillating at frequencies between 450 kHz and 4 MHz at power levels up to 100 kW, to directly heat the precursor kept at pressures over 100 atm to prevent decomposition. Crystals with XRD rocking curve FWHM of 27 arcsec have been produced [28]. Large boules of AlN crystals, with 25 mm diameter and 15 mm in length, have been fabricated by PVT using AlN powder and N_2 gas as precursors, in the temperature range between 2100 and 2300 °C and pressures between 200 and 900 Torr [29, 30]. Seeded growth using selected single crystals from unseeded growth resulted in larger high-quality single crystals up to 18 mm diameter [31]. These crystals, illustrated in figure 3, have typically XRD rocking curve FWHM of $\leqslant$40 arcsec.

Large area, ranging from 0.5 to 1.75 inch diameter, thick (0 0 0 1) AlN films have been deposited on Si and SiC substrates, at 1000–1100°C, by hydride vapour phase epitaxial (HVPE, a fast growth process) technique [32]. Freestanding (FS) films, accomplished by selective chemical etching of the sacrificial substrates, were used as seeds to grow AlN boules of a few millimetres of thickness. Wafers of 200–500 μm of thickness were sliced from the HVPE grown boules. After lapping and polishing, selected wafers were used as seeds for the growth cycle to improve the boules' crystalline quality. The typical value of the x-ray rocking curve FWHM of the (0 0 0 2) reflection is 700 arcsec, using a wide (10 mm × 1 mm) x-ray beam [33]. Despite the inferior crystalline quality, this approach can immediately provide large-area substrates for epitaxial growth. Recently, self-separated thick AlN films, grown by HVPE, have been realized by a three-step growth approach: namely, a thin low-temperature AlN film deposition at $<$1100 °C, higher temperature (1450 °C) treatment to form voids underneath the thin AlN film and growth of thick AlN layer at 1450 °C. FS crack-free 85 μm thick substrates were obtained during the cooling process. Despite this interesting result, more must be done to reduce the high concentration of dislocations typically on the order of 1.1×10^9 cm^{-2} [34].

2.2. *Growth of bulk and thick-film GaN*

Presently, there are several techniques under development for producing bulk GaN crystals including vapour phase transport, growth from supercritical fluids and growth from flux [35–39]. However, until recently, only high pressure–high temperature (*h*igh nitrogen *p*ressure *s*olution technique—HPS) and HVPE (a quasi-bulk growth process) methods have produced relatively large area substrates. In addition to these techniques, two recently developed approaches will be highlighted.

Unseeded GaN hexagonal platelets or needles (the latter formed under higher supersaturation conditions) have been grown by the HPS method from gallium melts saturated with 1 at% nitrogen at temperatures up to 1700 °C and nitrogen pressures of 20 kbar [40–42]. The supersaturation in the growth solution is achieved by employing a temperature gradient of 2–20 °C cm^{-1} along the axis of the crucible. The nitrogen dissolves at the hotter end of the crucible and the GaN crystallizes at the cooler end. For a typical process duration of 150–200 h relatively thin (∼300 μm thick) hexagonal platelets are grown with a rate of $<$2 μm h^{-1}, in the $\{1 0 \bar{1} 0\}$ directions (perpendicular to the *c*-axis), with maximum lateral dimensions up to 10 mm × 14 mm. The mechanism hindering the lateral growth of the platelets after 150–200 h can be related to changes in the mass transport mechanisms in the solution due to the presence of the crystal [43]. The (0 0 0 2) XRD rocking curve FWHM of these crystals are typically between 30 and 40 arcsec showing the presence of low angle (1–3 arcmin) boundaries separating grains of 0.5–2 mm in size [44]. High-resolution transmission electron microscopy studies indicate that threading dislocations commonly observed in heteroepitaxial GaN films are not detected in the HPS bulk GaN, and dislocation densities as low as 10^2 cm^{-2} are frequently observed. Due to the slow growth rate (∼1–2 μm h^{-1} along [0 0 0 1] and ∼50–100 μm h^{-1} along $[1 0 \bar{1} 0]$) and the limited final substrate size (hexagonal plates of 10–20 mm in the longest direction with 0.1 mm of thickness, figure 4) achieved by this self-nucleated technique, a modified approach using large FS seeds produced by HVPE has recently been implemented [45]. Preliminary results of this approach show small growth rates, 1–3 μm h^{-1}, for both the Ga and N faces, and no growth was verified in the direction perpendicular to the basal plane. These observations raise questions about the use of such an approach for the growth of large GaN boules.

Ammonothermal growth of bulk GaN is a modification of the hydrothermal growth technique developed to grow high-quality quartz [46]. The latter uses water while the former uses ammonia (NH_3) as the polar solvent. Ammonothermal growth requires the use of autoclaves with a large volume of ammonia (36–58%), temperature gradients between 500 and 700 °C and pressures in the range 150–400 MPa. Acidic (e.g. NH_4Cl) and basic (e.g. $NaNH_2$ or KNH_2) mineralizers have been employed. The polycrystalline GaN or liquid Ga is mixed with the mineralizer in the feedstock reservoir, while the GaN seeds are placed in the higher temperature zone, in the case of basic mineralizer, or in the colder zone, if an acidic mineralizer is employed, of the autoclave. The growth rate is typically 0.1 mm per day [47]. This rate is about

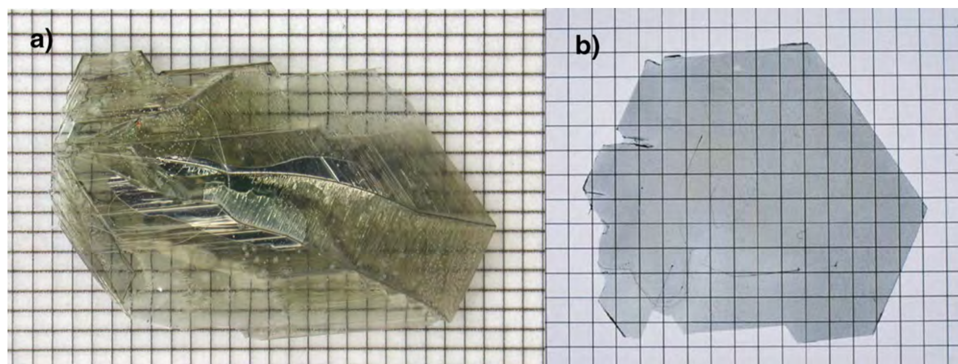

Figure 4. Large GaN crystal grown by HPS technique: (*a*) as grown cystal and (*b*) epi-ready wafer, after mechanical and chemical mechanical polishing. (Courtesy of M Bockowski, UNIPRESS, PAS, Poland.)

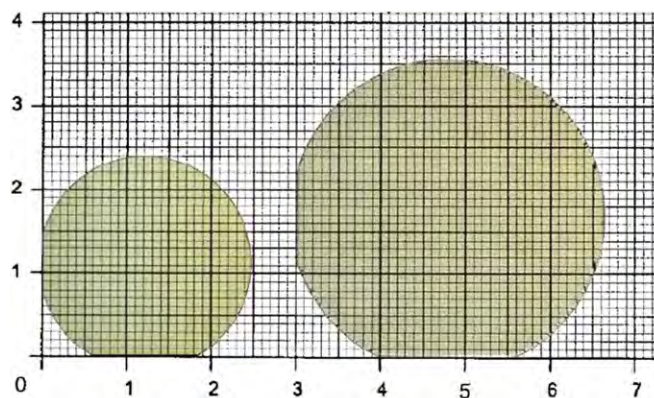

Figure 5. Photograph of 1 and 1.5 inch diameter wafer grown by basic mineralizer ammonothermal technique. (Courtesy of R Dwilinski, Ammono, Poland.)

20 lower than quartz-hydrothermal and about 25 lower than GaN-HPS growth techniques. However, the scalability of the autoclaves, the very large number of seeds that can be placed simultaneously and the capability to sustain growth for many hundreds of hours can overcome the small growth rate demerit. Previously, this technique succeeded only in growing needles and platelets of a few millimetres in size, but recently a few reports demonstrate that large samples could be grown on FS HVPE GaN seeds [48–51]. Recently, Dwilinski and co-workers reported the growth of 25–38 mm diameter wafers (figure 5) characterized by low dislocation density, typically on the order of 5×10^3 cm^{-2}, with a very narrow XRD (0 0 0 2) rocking curve (FWHM of 17 arcsec) and curvature radii between 100 and 1000 m [52, 53]. To achieve such impressive results, starting from micrometre-sized crystals, took over 15 years. Presently, high crystalline quality *c*-plane wafers and *m*-plane slab (17×8 mm^2) substrates are produced [53, 54].

Yamane and co-workers developed a Na-base flux method at elevated pressures (5–10 MPa) and intermediate temperatures (600–900 °C) to grow self-nucleated prismatic and platelets of GaN up to 10 mm size, in the longest direction [55]. Despite the good crystalline quality, verified by XRD peak FWHM of 25–55 arcsec for the (0 0 0 2) reflection, the formation of polycrystalline layers prevented the growth of larger crystals. Recently, it has been found that the addition of 0.5 at% of carbon powder in the starting metal Ga and Na precursors suppresses the parasitic nucleation of GaN crystals in the Na flux method. As a result, a 3 mm thick GaN film was deposited by liquid phase epitaxy (LPE) on a 2 inch diameter thin GaN film grown on sapphire by organic metallic vapour phase epitaxy (OMVPE). The estimated growth rate was 20 μm h^{-1}, which is considerably larger than that of the ammonothermal technique [56]. Despite the high concentration of dislocations in the GaN film a significant reduction in the dislocation density occurs in the overgrown layer due to the formation of dislocation bundling. It was verified that three-fourths of the sample has a dislocation density of about 10^2 cm^{-2} (figure 6) and XRD rocking curve FWHM for the (0 0 0 2) reflection of 28 arcsec [57].

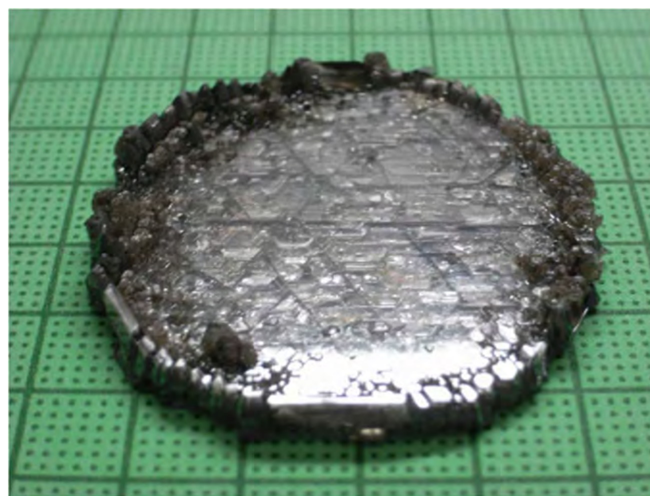

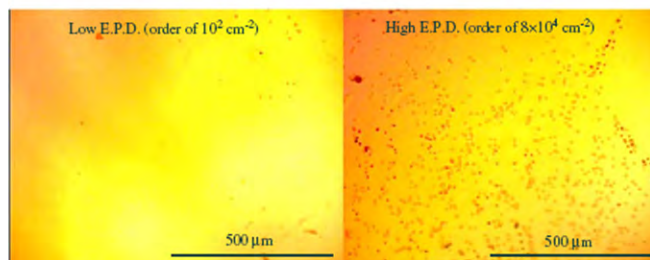

Figure 6. Picture of a 3 mm thick 2 inch GaN wafer grown by LPE based on the Na flux method. Regions with dislocation densities of about 10^2 cm^{-2} and 10^4 cm^{-2} are observed across the sample surface. (Courtesy of Y Mori, DEEIE, Osaka University, Japan.)

Industrial production will require a low-cost technique operating under low to moderate pressure and temperature growth conditions. Presently, a new approach to grow GaN from solution, at a nitrogen pressure of ∼0.24 MPa and a temperature of about 800 °C is under development. Self-nucleated high-quality crystals of ∼10 mm^2 area and 300 μm thickness as well as homoepitaxial films have been demonstrated. These crystals yielded record low XRD rocking curves and optical phonons FWHM [58].

The HVPE growth processes of III–V/N have been developing for about four decades [59]. Presently, GaN wafers of 2 and 3 inch diameter and thickness of 100–300 μm, with dislocation density typically between 10^6 and 10^7 cm^{-2} are commercially available. These thick and crack-free GaN films are deposited on *c*-plane sapphire substrates, the sacrificial substrate of choice [60–63]. The substrates are placed on a 1030 °C horizontal susceptor of a hot-wall HVPE reactor. Ga metal and HCl are pre-reacted to form GaCl gas, which is transported by nitrogen carrier gas to the hot growth zone where it reacts with NH_3 and deposits GaN on the (0 0 0 1) sapphire substrate. For a V/III ratio from 20 to 35, a growth rate between 30 and 100 μm h^{-1} can be reproducibly achieved. These thick layers can be removed from the sapphire substrates by laser-assisted lift-off or by void-assisted self-separation [60–63]. The growth surfaces of the FS GaN templates are extremely rough with large number of hillocks, and are inadequate for homoepitaxial growth. Flat, smooth surfaces are obtained after mechanical polishing, which introduces subsurface damage extending up to 4000 Å below the surface. The polished growth surfaces (Ga-face) are reactive ion etched (RIE) to remove the damage [61]. Chemical mechanical polishing techniques have been developed to yield smooth epi-ready surfaces [64]. Selected wafers have been placed in a vertical HVPE reactor to grow GaN boules with lengths up to 0.5 inch. GaN boules of 2 inch diameter have also been grown directly on AlN/sapphire templates, with a growth rate of about 200 μm h^{-1} [65]. These boules can be sawn to produce polar (*c*-face {0 0 0 1}) and non-polar (*a*-face $\{1\,1\,\bar{2}\,0\}$ and *m*-face $\{1\,\bar{1}\,0\,0\}$) substrates. The crystalline qualities of these substrates have been improving systematically, and XRD rocking curves with FWHM around or less than 100 arcsec can be obtained [64, 65]. Despite different approaches implemented to reduce the high dislocation density, the lowest values are still in the range 10^5–10^6 cm^{-2}, the theoretical limit for heteroepitaxial growth on non-native substrates.

Thick HVPE GaN substrates have also been realized on GaAs (1 1 1) using a two-step growth process, such as selective epitaxial overgrowth, which is basically accomplished by depositing a low-temperature GaN buffer layer prior to the growth of the high-temperature film deposited at 1000 °C. These GaN films can be easily removed from the substrates by selective etching [66]. Films with a thickness of 1.5 mm are characterized by regions of ∼50 × 400 μm^2 with a dislocation density as low as 3×10^4 cm^{-2} and larger regions with densities of 1×10^7 cm^{-2} [67]. Using these substrates for device fabrication requires special handling of the regions with low dislocation densities.

Low dislocation density HPS GaN substrates were used for seeded HVPE growth in an attempt to produce high-quality thick substrates. It was observed that a high concentration of dislocations was introduced in the HVPE homoepitaxial film at thicknesses between 50 μm and 100 μm for n-type conducting and resistive substrates, respectively [68]. To prevent the incorporation of these dislocations, the HVPE growth was interrupted before reaching the critical thickness and the HPS substrate was removed. The thin FS HVPE film was placed back in the reactor to grow a few millimetres thick substrate characterized by low dislocation density and sharp XRD rocking curve [68]. Despite the improved crystalline quality of the HVPE crystal, no lateral growth was observed indicating that this multiple-step approach is not adequate for industrial production.

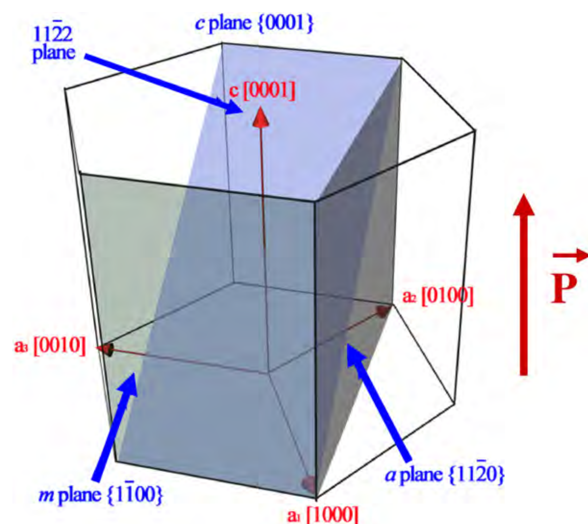

Figure 7. Schematic diagram of the polar, non-polar and semi-polar GaN planes curently used for homoepitaxial growth. The polarization ***P*** is indicated.

3. Structural properties of III-nitride substrates

The lattice parameters of semiconductors are affected by various factors, such as stoichiometry, excess of free carriers, high concentration of point and extended defects and external stresses (e.g. heteroepitaxial layers). Therefore, III-nitride lattice parameters are still not completely determined [70]. The hexagonal (2H) phase of bulk AlN and GaN (wurtzite structure) belongs to the space group C_{6v}^4 or $P6_3mc$, consisting of two interpenetrating hexagonal, close-packed lattices (figure 1). The III-nitrides commonly have their faces perpendicular to the (0 0 0 1) *c*-axis. These faces, {0 0 0 1} basal planes, are polar with either nitrogen or aluminium/gallium termination. These characteristics play important roles in the physical and chemical properties of the III–V/N. The use of polar, non-polar or semi-polar substrates (simplified schematic represented in figure 7) could affect growth mode and rate, and impurity and defect incorporation. In addition, anisotropies of physical properties can be conveniently used for device applications. There has been considerable controversy with regard to the identification of GaN face polarities [71, 72]. Presently, there is a common agreement that the nitrogen-terminated face is chemically

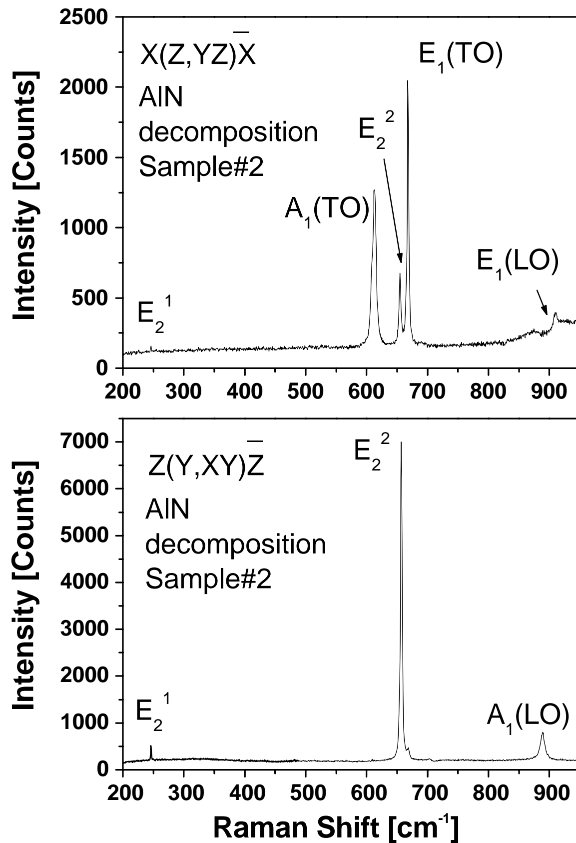

Figure 8. Room temperature polarized Raman spectra of a high-quality bulk AlN [77]. The letters inside the brackets represent the incident and the scattered light polarization, while the letters outside the brackets represent the direction of the incident and scattered light. (Reproduced with permission.)

active, whereas the gallium-terminated face is inert. Therefore, the face polarity can be easily identified by selective chemical etching techniques [73].

The AlN and GaN wurtzite structure has two molecules per unit cell. Group theory predicts eight zone-centre optical modes, namely $1A_1$ (TO), $1A_1$ (LO), $2B_1$, $1E_1$ (TO), $1E_1$ (LO) and $2E_2$. The two B_1 modes are optically inactive, but all of the six allowed modes have been observed by Raman scattering (RS) spectroscopy [74, 75].

The room temperature first-order Raman spectra of a high crystalline quality bulk AlN, measured at two different sample orientations and light polarizations, are represented in figure 8. The Raman lines for the allowed modes A1(TO), E1(TO), E_2^2, A1(LO) and E1(LO) are observed at 608.5 cm^{-1}, 667.2 cm^{-1}, 655.1 cm^{-1}, 888.9 cm^{-1} and 909.6 cm^{-1}, respectively. The peak positions and record small linewidths of the phonon lines indicate that low defect and stress free crystals can be produced. A complete discussion of the RS study of bulk AlN is presented elsewhere [76]. The GaN Raman shift for the allowed modes A1(TO), E1(TO), E_2^2, A1(LO) and E1(LO) are 534 cm^{-1}, 559 cm^{-1}, 569 cm^{-1}, 734 cm^{-1} and 740 cm^{-1}, respectively. Analyses of the peak positions and linewidths of the observed first-order phonons confirm the good crystalline quality and lower biaxial stress of the wurzite FS HVPE GaN substrates [77].

4. Optical and electronic properties of III-nitride substrates

Wurzite GaN has the conduction band minimum at the centre of the Brillouin zone (Γ-point, $k = 0$), and has a Γ_7-symmetry with quantum number $J_Z = 1/2$. The valence band of 2H-GaN has its maximum also at the Γ-point, which results in a direct fundamental bandgap. As a result of the crystal-field (Δ_{cr}) and spin–orbit (Δ_{so}) coupling, the top of the valence band splits into three sub-bands with symmetries Γ_9, Γ_{7upper} and Γ_{7lower}, which are traditionally labelled A, B and C, respectively [77–83]. Reported calculations of AlN generally agree that Δ_{cr} is negative and promotes the Γ_{7upper} band to a higher energy than the Γ_9 band. However, there is considerable disagreement with regard to the calculated values for effective masses, crystal field and spin–orbit splitting [79, 83, 85].

4.1. Bulk and thick-film AlN

Despite the large concentration of residual oxygen in AlN, typically between $\sim 1 \times 10^{18}$ and 1×10^{21} cm^{-3}, it is still semi-insulating (SI) at room temperature. This is due to the fact that most of the oxygen is not incorporated as a substitutional shallow donor, but as an impurity forming complexes with point and extended defects, which are located deep in the gap and behaving as compensating centres [27, 86–89]. Most of the oxygen incorporated in single crystal bulk AlN originates from the Al precursor. High temperature annealing and sintering are required to reduce the high initial oxygen concentration [90]. Low oxygen content bulk AlN has a record high thermal conductivity of 270 $W\,mK^{-1}$ [27]. Resistivities as high as 8×10^{10} Ω cm and 1×10^{10} Ω cm at 300 °C and 750 °C, respectively, have been reported for single crystal bulk AlN [91]. AlN wafers grown by HVPE show a typical resistivity exceeding 10^8 Ω cm at room temperature and 10^6 Ω cm at 500 K [33].

Figure 9 shows the low-temperature cathodoluminescence (CL) spectrum from 2.0 eV to approximately 6.2 eV of an *a*-face bulk AlN sample reported in [87], which has a relatively low oxygen content. In addition to an intense sharp emission line, the near band edge (NBE) emission around 6.0 eV, two broad and featureless bands with peaks near 3.5 eV (VB) and 4.4 eV (UVB) are also observed. These broad bands have been previously associated with oxygen impurities [86, 87]. The high-resolution CL spectrum of the NBE emission is represented in the inset of figure 9. The continuous line is the best fit to the experimental data, represented by the open circles, using Lorentzian line shapes. The intensity and the sharpness of the lines attest to the high crystalline quality of the sample. Thermal ionization studies of the NBE emission strongly suggest that the most intense line at 6.010 eV is associated with recombination processes involving the annihilation of excitons, with hole from the lowest energy valence band (FX_A), bound to a shallow unknown neutral impurity, with an exciton binding energy of about 15 meV [92]. The lines at 6.026 and 6.041 eV are observed up to 150 K, which may be related to the annihilation of free excitons [92]. Detailed optical reflectance studies performed on *a*-face and

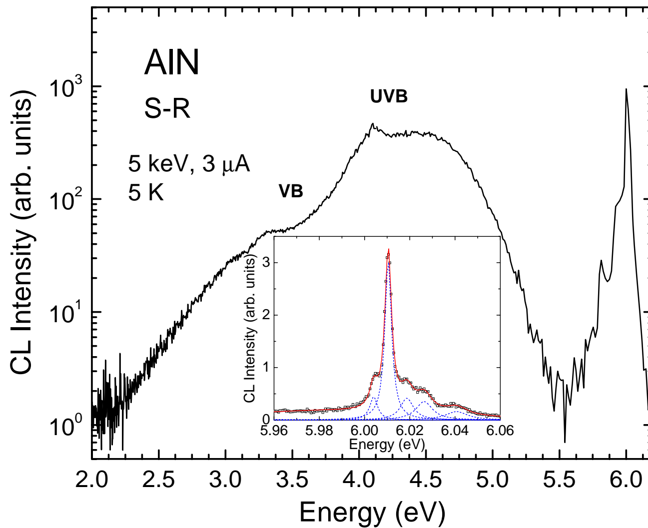

Figure 9. 5 K CL spectrum of an *a*-plane AlN sample fabricated by the S–R technique. The nature of NBE emission and the two broad emission bands are discussed in the text [92]. The figure inset shows the high-resolution CL spectrum of the NBE emission. The assignments of these lines are discussed in the text. (Reproduced with permission.)

c-face oriented bulk AlN crystals identified and measured the energy of the free excitons 'A', 'B' and 'C', FX_A, FX_B and FX_C, respectively. In addition, these experiments yielded the spin–orbit and crystal-field splitting values of $\delta = 36$ meV and $\Delta = -225$ meV, respectively [93]. These results, obtained by using recently measured accurate dielectric constant values, confirmed the theoretical prediction of negative value of the crystal-field splitting [94]. Recently, detailed studies of temperature dependence of absorption performed in similar samples show that the room temperature bandgap of bulk AlN is about 6.0 eV [95]. This value is considerably smaller than the previously reported value of 6.3 eV.

CL measurements performed on samples fabricated by RF-assisted PVT and HVPE show the same spectral features observed in the CL spectra of samples grown by the S–R technique, despite variations of the relative intensity of the various emission bands present in the luminescence spectra. This observation strongly suggests the pervasive character of impurities and defects incorporated in AlN independent of the growth technique of choice [28, 33, 87]. Therefore, it is very important for the progress of this material to find out about the chemical nature and crystalline structure of the defects to achieve control of the optical and electronic properties of bulk AlN.

4.2. Bulk and thick-film GaN

Bulk GaN crystals grown by the HPS method are typically n-type and degenerate, with temperature-independent carrier concentrations and mobilities typically between 10^{19} cm^{-3} and 10^{20} cm^{-3} and 30 cm^2 V^{-1} s^{-1} and 90 cm^2 V^{-1} s^{-1}, respectively [96]. This result is consistent with the strong LO-phonon/conduction electron–plasmons coupling mode observed in the Raman spectra [96]. Oxygen is assumed to be the shallow donor responsible for the observed high concentration of free electrons [97]. The low-temperature PL spectra of such samples typically show an intense broad band with a peak around 2.25 eV and a weak and relatively broad NBE emission with a peak near 3.5 eV [98]. The NBE emission higher energy shift results from the large concentration of free carriers causing the semiconductor–metal transition, the so-called Burnstein–Moss effect [99, 100].

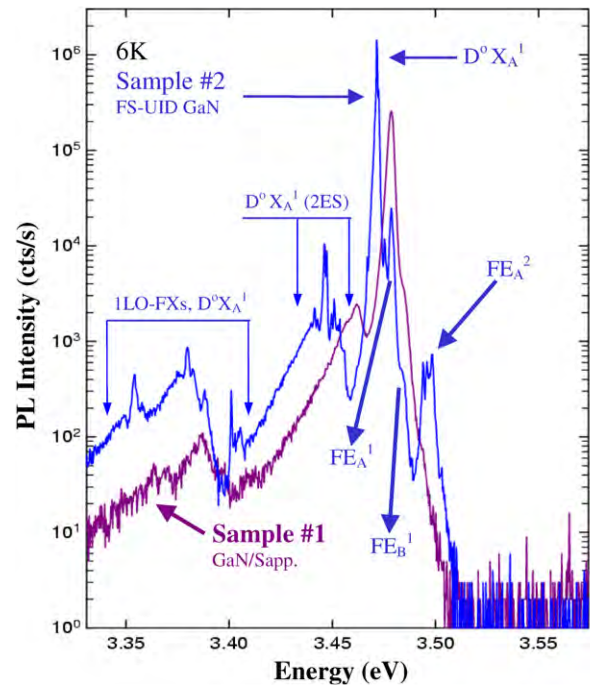

Figure 10. 6 K PL spectra of a ∼12 μm thick heteroepitaxial GaN film (sample 1) and of a ∼150 μm thick FS GaN substrate (sample 2) [102]. The presence of a variety of sharp excitonic lines in this spectral region indicates the high crystalline quality of both samples. (Reproduced with permission.)

Unintentionally doped (UID) thick FS HVPE GaN films are also typically n-type, but with much lower background free-electron concentration than HPS bulk GaN. Detailed electrical transport experiments of high-quality samples yield a room temperature carrier mobility of 1245 cm^2 V^{-1} s^{-1} and a carrier concentration of 6.7×10^{15} cm^{-3} for a compensating centre concentration of 1.7×10^{15} cm^{-3} [101]. Assuming an idealistic reduction of two orders of magnitude of the background donors and acceptors, to keep the same compensation level, the maximum mobility at room temperature is expected to reach 1350 cm^2 V^{-1} s^{-1} [101].

Low-temperature PL spectra of similar UID FS HVPE GaN films typically show intense recombination emission lines associated with annihilation of excitons bound to neutral donors (D^oX) and their phonon replicas (nLO-D^oX). Also commonly observed are weak zero-phonon lines from shallow-donor/shallow-acceptor pairs (DAP) recombination and their phonon replicas (nLO-DAP). Figure 10 shows the PL spectra of a ∼12 μm thick heteroepitaxial film (sample 1) and a ∼150 μm thick FS substrate (sample 2) described in [102, 103]. The spectrum of sample 2 shows, in the 3.52–3.46 eV region, emission lines related to the excited state of the free-exciton A (FX_A^2), the ground state of the free-exciton B (FX_B^1), the ground state of the free-exciton A (FX_A^1)

and the dominant exciton bound to a neutral donor (D^oX). Around 3.45 eV, we detect the so-called two-electron satellite (2ES) spectrum resulting from the recombination processes in which the neutral donors are left in an excited state after the exciton annihilation. Note that for energies below 3.42 eV, we observe the one-phonon replicas of all features listed above. The PL spectrum of sample 1 shows most of the features observed in the spectrum of sample 2. However, these features are broader and smeared, and shifted to higher energies due to inhomogeneous broadening and compressive strain, respectively, caused mostly by the substrate lattice mismatch [102]. A combination of low-temperature high-resolution PL and IR absorption spectroscopies with high sensitivity SIMS studies identified Si and O as the two pervasive and dominating shallow donors in GaN. The impurities' binding energy values of 30.19 ± 0.01 meV and 33.21 ± 0.01 meV were obtained for Si and O, respectively [103–105]. Although n-type bulk substrates are convenient for the fabrication of optical devices, SI substrates are the most desirable for the fabrication of high-frequency devices. Material scientists have employed different approaches, adequate for each growth technique, to reduce the background carrier concentration by controlling the growth conditions and/or doping with impurities to provide the necessary concentration of compensating centres.

Degenerate HPS bulk GaN substrates, if doped during the growth with Mg, show increasing resistance with increasing doping concentration. For Mg doping concentrations between 10^{19} and 10^{20} cm^{-3}, resistance as high as 10^8 Ω at about 600 K was observed [105]. Infrared transmission measurements performed on such samples show no free-carrier absorption and improved optical properties.

Nominally undoped FS HVPE GaN, which also are typically n-type with background carrier concentration $\leqslant 1 \times 10^{17}$ cm^{-3}, can be grown SI by using intentionally introduced transition metal impurities during the growth to compensate the residual donors. Iron concentrations on the order of 1×10^{18} cm^{-3} are sufficient to compensate unintentionally incorporated impurities and native defects. The resistivities of such samples measured at room temperature were larger than 10^{10} Ω cm [107]. Zn doping, with concentrations ranging between 10^{18} and 10^{20} cm^{-3}, was also successfully employed to grow SI GaN films with resistivities of 10^{12} Ω cm at 300 K and 10^9 Ω cm at 500 K [108].

5. Optical and electronic properties of homoepitaxial III-nitride films

The viability of improved quality bulk AlN and bulk and thick FS films of GaN substrates opens the possibility of depositing high-quality device grade homoepitaxial layers and ternary and quaternary epitaxial alloy layers for the fabrication of high performance and high yield devices.

5.1. Homoepitaxial AlN films

UID homoepitaxial films deposited by metal organic chemical vapour deposition (MOCVD) on high-quality S–R bulk AlN substrates misaligned 10° from the *c*-axis, with a

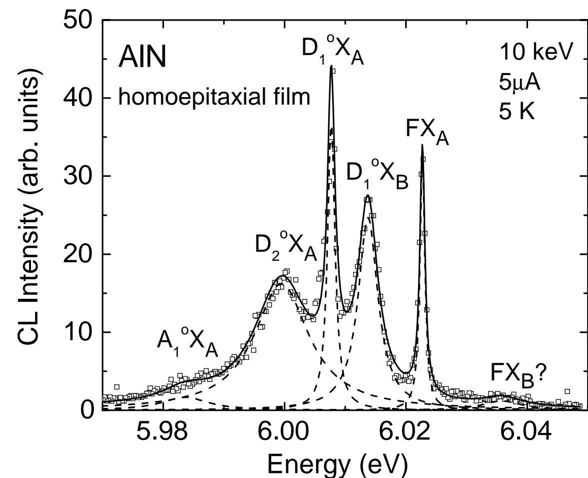

Figure 11. High-resolution CL spectra of a MOCVD AlN film deposited on a sublimation AlN substrate [110]. The details of the line assignments are presented in the text. (Reproduced with permission.)

nominal thickness of 0.5 μm and surface roughness typically of 0.21 nm, have been investigated by variable-temperature high-resolution CL spectroscopy [109, 110]. The NBE CL spectrum measured at 5 K, represented in figure 11, shows six individual lines assigned to recombination processes involving the annihilation of free excitons and excitons bound to neutral donor and acceptor impurities. These assignments rely on detailed thermal quenching studies [109]. These lines are considerably narrower than those previously observed in the bulk AlN substrate, which indicates the improved structural and optical properties of the homoepitaxial layer. Comparison of the CL spectrum of this homoepitaxial film with the optical reflectance spectrum of an *a*-face bulk AlN crystal, represented in figure 12, confirms the assignments of the lines associated with recombination processes involving ground state (FX_A) and excited state (FX_A^2) free excitons. However, this reflectance study does not support the assignment of the small peak at about 6.036 eV to recombination process associated with the annihilation of FX_B, which is represented by 'FX_B?' in figure 11 [93, 109]. The energy separation between FX_A and FX_A^2 emission lines yields a free-exciton binding energy of 48 meV. Note also that the binding energy of excitons to neutral donors is about three times larger than that observed for GaN. It is also important to point out that the spectral energy position of the exciton bound to the pervasive donor in bulk AlN is smaller than that reported for Si-doped heteroepitaxial films. This indicates that Si is not the pervasive shallow donor in bulk AlN [111]. One can speculate that oxygen or nitrogen vacancy may be the unknown shallow donor in AlN. UID homoepitaxial HVPE films of about 2 μm have also been successfully deposited on FS wafers grown by HVPE. The increased ratio of the intensity of NBE emission lines to the intensity of the deep emission bands of the homoepitaxial layer in comparison with the ratio of these bands in the HVPE substrates strongly suggests the improved quality of the homoepitaxial layers [33].

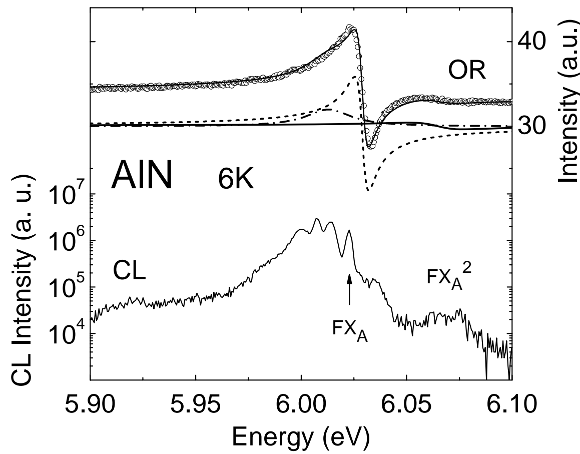

Figure 12. Optical reflectivity spectrum of an a-face bulk AlN crystal grown by S–R. The full curve is the best fit of the experimental data represented by hollow symbols. The CL spectrum of the homoepitaxial film represented in figure 11 is also depicted to support the assignment of FX_A and FX_A^2 recombination processes. (Reproduced with permission.)

5.2. *Homoepitaxial GaN films*

Epitaxial films have been deposited on bulk HPS GaN substrates by MBE, using on surface cracked ammonia as nitrogen precursor, and MOCVD methods [112, 113]. Detailed low-temperature PL and reflectance measurements were performed on the MOCVD film to identify the nature of the lines observed in the NBE emission spectral region [113]. The lines assigned to the recombination process involving excitons bound to shallow donors have FWHM of about 100 μeV, indicating the high crystalline quality of the homoepitaxial layer. XRD experiments performed on similar structures indicate that the homoepitaxial film has a lower lattice parameter c than the substrate, which typically has room temperature free-carrier concentration in excess of 5×10^{19} cm^{-3} [114]. Recently, similar experiments were carried out on 2 μm thick GaN films deposited by MOCVD on SI ammonothermal substrates. Narrow lines associated with the annihilation of excitons bound to neutral donors and acceptors were observed in the low-temperature PL spectra [54]. UID and Si-doped ($\leqslant 1 \times 10^{17}$ electron cm^{-3}) homoepitaxial layers were deposited on FS HVPE GaN substrates with a nominal surface roughness of about 5 nm by low-pressure MOCVD. Films with a thickness of about 5 μm were characterized by a growth surface roughness of about 0.2 nm RMS and reduced threading dislocation density, as compared with the substrate [115]. The spectrum in figure 13 marked as Homo-UID, measured on the UID homoepitaxial film, shows a reduction in the total intensity of the neutral donor-bound exciton related emissions and a relative decrease in intensity to the free-exciton line. The lower energy side of the neutral donor-bound exciton emission band is also reduced, suggesting that the dominant donor is at the higher energy side of this band. This is consistent with the reduction in the concentration of the neutral donor background in the UID homoepitaxial film. The PL spectrum of the Si-doped film is characterized by a

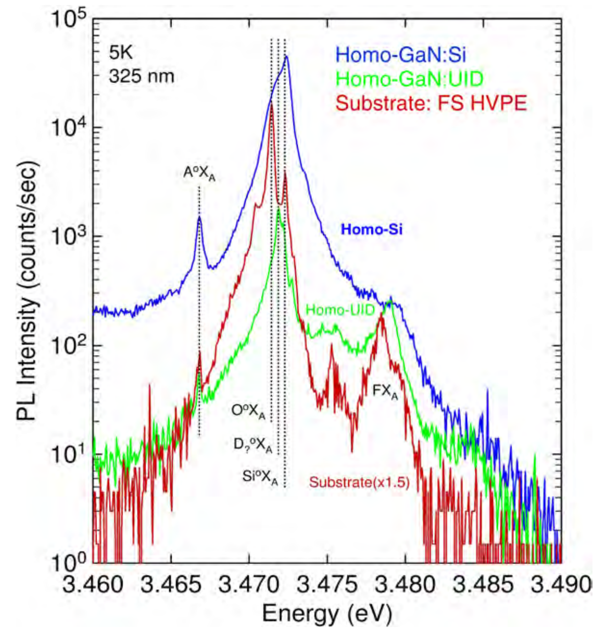

Figure 13. High-resolution PL spectra of two MOCVD homoepitaxial GaN films, an UID (Homo-UID) and a Si-doped, deposited on FS HVPE substrates, and a FS HVPE substrate [115]. The assignments of the lines associated with excitonic recombination processes are discussed in the text. (Reproduced with permission.)

larger increase on the high-energy side of the neutral donor-bound excitons, indicating that Si is in fact the shallower donor in GaN [115]. Similar results were observed on UID and Si-doped GaN epitaxial films grown by molecular beam epitaxial (MBE) technique on FS HVPE substrates [116]. The UID film had Si background of 4.5×10^{14} cm^{-3} (Si detection limit) and O background of $\sim 3.3 \times 10^{16}$ cm^{-3}. The low-temperature PL of this film, depicted in figure 14, clearly shows that the line assigned to excitons bound to neutral Si impurities is missing. Also missing are the lines assigned to the Si impurity in the 2ES spectrum, in the spectral region between 3.445 and 3.455 eV. These observations undoubtfully confirm that Si is the shallowest pervasive donor in GaN [103, 105]. In addition, it should be mentioned that the line assigned to the recombination process of excitons bound to a shallow unknown acceptor is missing. This strongly supports the assumption that Si on the nitrogen sublattice site is the unknown shallow acceptor in GaN [117, 118].

6. Bulk nitride based optoelectronic and electronic devices

Native nitride substrates, characterized by low concentration of extended defects and controlled electrical properties, are the required platform for epitaxial growth of the next generation III-nitride based devices. It has been pointed out above that large-area III–V nitride substrates with improved crystalline quality are under development by a number of research groups in companies and universities, and promising results have recently been reported. Some of these improved quality substrates are commercially available at relatively high cost.

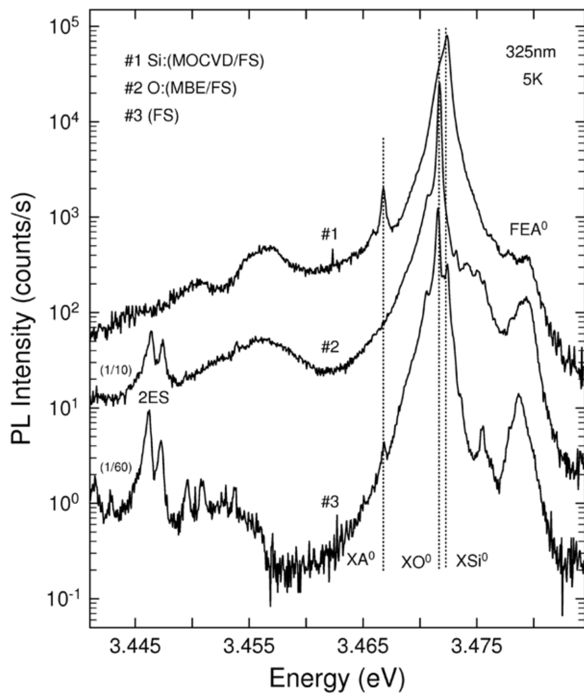

Figure 14. Low-temperature PL spectra of an unintentionally oxygen doped homoepitaxial GaN film deposited by MBE on a FS HVPE substrate [116]. The PL spectra of the FS HVPE substrate and Si-doped epitaxial samples, represented in figure 13, are also depicted. (Reproduced with permission.)

However, it is expected that the improved growth technology and increased productivity will drive the substrate cost down as experienced in other material systems. To illustrate the advantage of using bulk nitride substrates for devices fabrication, a few examples of devices are highlighted below.

Optoelectronic device applications have been the driving force for III-nitride research. GaN and InGaN can be conveniently tailored to emit or detect light in the spectral range between near UV and red. Therefore LED, LD and photodetector devices based on these two materials deposited on foreign substrates have been intensively investigated, and presently largely commercialized. However, the needs of optical devices with a higher quantum efficiency require the use of native substrates with dislocation density 4–5 orders of magnitude lower than these heteroepitaxial templates. Despite the typical dislocation density of mid-10^6 cm^{-2}, FS HVPE substrates have been successfully used for this application [119]. The wurzite III-nitride semiconductors have large spontaneous and piezoelectric fields on the [0 0 0 1] polar direction as indicated in figure 7. While these fields are useful in the formation of a two-dimensional electron gas, they are detrimental to optical devices because they introduce a large separation between electron and hole wave functions, leading to a reduction in the device quantum efficiency. Recently, various research groups demonstrated that higher quantum efficiency LED and LD can be fabricated on non-polar m- and a-plane HVPE substrates, which do not show the characteristic blue shift observed on basal-plane structures under high driving currents [120–123]. It was reported that the incorporation of In into the InGaN wells is significantly smaller for non-basal plane substrates, which makes it more difficult to fabricate green light emitting LED and LD [124]. Despite this observation, recently 531 nm emission was obtained from a InGaN LD fabricated on semi-polar $\{20\bar{2}1\}$ FS HVPE substrates [125]. LDs have also been fabricated on HPS substrates by MOCVD and MBE techniques, which have lower dislocation densities than the HVPE substrates. Under CW operation a maximum power of 215 mW can be achieved in the wavelength range 405–420 nm [126]. As mentioned above, the epitaxial films deposited on polar substrates result in the formation of a two-dimensional electron gas at the heteroepitaxial film–substrate interface, which is required for the fabrication of high electron mobility transistors (HEMTs). Room temperature Hall measurements verified electron mobilities of 1750 $\mathrm{cm^2\,V^{-1}\,s^{-1}}$ and sheet densities of 1.1×10^{13} cm^{-2}. AlGaN/GaN HEMTs with output power densities of 4.8 $\mathrm{W\,mm}^{-1}$ at 10 GHz and off-state breakdown voltages up to 200 V were realized on HVPE GaN substrates [127]. Another potential application for bulk GaN is the fabrication of ultrafast rectifiers. Preliminary results demonstrate that GaN-based Schottky diodes with breakdown fields of $\sim$5.5 $\mathrm{kV\,cm}^{-1}$ and a recovery time of less than 20 ns can be realized [128].

Only recently, sublimation grown high-quality bulk AlN has become available for device fabrication. It is expected that devices such as solar blind detectors, deep-UV LEDs and HEMTs, among other devices, fabricated on bulk AlN will show considerable improvement in performance and yields. As a proof of case AlGaN-based LED fabricated on bulk AlN substrates, with electroluminescence emission peak at 300 nm, yielded an output power four-fold higher than that from a nominally identical device on sapphire substrates [129]. InGaN-based current injection lasers, emitting in the spectral range 368–372 nm with peak power on the order of 300 mW, have been realized. In addition, optically pumped AlGaInN-based heterostructures successfully reach laser emission at 308 nm [128]. A concern is the increasing concentration of extended defects in the AlGaN film for thicknesses above 40 nm, the critical film thickness. However, recent pseudomorphic AlGaN films, with a low dislocation density and thickness exceeding the critical limit, were successfully grown [129].

7. Closing remarks

The morphological, structural, optical and electronic properties of bulk and thick FS HVPE films of AlN and GaN grown by a number of techniques have been reviewed. The homoepitaxial layers deposited on some of these substrates show improved structural, optical and electrical properties as compared with that of heteroepitaxial films. However, epitaxial-ready surface is still an important issue to be addressed in detail. Chemical mechanical polishing and reactive ion etching (RIE) have been used to achieve epitaxial-ready surfaces with 0.3–0.5 nm RMS of roughness, but these processes have not yet been fully developed. The well-established technology for the fabrication of LEDs and HEMTs on sapphire and SiC, and the availability and relative low cost

of these substrates ensure that these substrates will remain the substrate of choice for the foreseeable future. Therefore, bulk or quasi-bulk III-nitride substrates may play a role in the fabrication of devices that require high power density and low leakage current such as SSL, LD, and high-frequency and/or high-power devices. The limited availability and size of the III-nitride substrates and their present high commercial cost are serious limiting factors for a generalized use of these substrates for the fabrication of optical and electronic devices.

Presently, an increasing number of R&D institutions are seeking commercialization of AlN and GaN substrates grown by a variety of techniques. It is expected that in the long term, after a few growth techniques and related processes become fully developed, the present high cost of these substrates will drop considerably and high-quality substrates will be available, as experienced in other semiconductor material systems.

Acknowledgments

Dr E R Glaser and Dr B N Feigelson are gratefully acknowledged for critical reading of this paper.

References

[1] Yoshida S, Mizawa S and Gonda S 1983 *Appl. Phys. Lett.* **42** 427
[2] Amano H, Sawaki N, Akasaki I and Toyoda T 1986 *Appl. Phys. Lett.* **48** 353
[3] Nakamura S 1992 *Japan. J. Appl. Phys.* **31** L139
[4] Nakamura S and Fasol G 1997 *The Blue Laser Diode* (Heidelberg: Springer)
[5] Mishra U K, Parikh P and Wu Y-F 2002 *Proc. IEEE* **90** 1022
[6] Perlin P, Jauberthie-Carillon C, Itié J P, Miguel A S, Grzegory I and Polian A 1992 *Phys. Rev.* B **45** 83
[7] Ueno M, Onodera A, Shimomura O and Takemura K 1992 *Phys. Rev.* B **45** 10123
[8] Ueno M, Yoshida M, Onodera A, Shimomura O and Takemura K 1994 *Phys. Rev.* B **49** 14
[9] Mizuta M, Fujieda S, Matsumoto Y and Kawamura T 1986 *Japan. J. Appl. Phys.* **25** L945
[10] Lima A P, Tabata A, Leite J R, Kaiser S, Schkora D, Schöttker B, Frey T, As D J and Lischka K 1999 *J. Cryst. Growth* **201–202** 396
[11] Tabata A, Lima A P, Teles L K, Scolfaro L M R, Leite J R, Lemos V, Schöttker B, Frey T, Schkora D and Lischka K 1999 *Appl. Phys. Lett.* **74** 362
[12] Powel R C, Lee N E, Kim Y W and Green J E 1993 *J. Appl. Phys.* **73** 189
[13] Lei T, Fanciulli M, Molnar R J, Moustakas T D, Graham R J and Scanlon J 1991 *Appl. Phys. Lett.* **59** 944
[14] Paisley M J, Sitar Z, Posthill J B and Davis R F 1998 *J. Vac. Sci. Technol.* A **7** 701
[15] Van Vechten J A 1973 *Phys. Rev.* B **7** 1479
[16] Grzegory I, Krukowski S, Jun J, Boækowski M, Wróblewski M and Porowski S 1994 *AIP Conf. Proc.* **309** 565
[17] Karpinski J, Jun J and Porowski S 1984 *J. Cryst. Growth* **66** 11
[18] Slack G A 1998 *Mater. Res. Soc. Symp. Proc.* **512** 35
[19] Chase M W 1998 *NIST-JANAF Thermochemical Tables* 4th edn (American Chemical Society and American Institute of Physics) p 130
[20] Cox G A, Cummins D O, Kawabe K and Tredgold R H 1967 *Phys. Chem. Solids* **28** 543
[21] Krukowska-Fulde B and Niemyski T 1970 *Electron. Technol.* **3** 3
Ishii T, Sato T and Iwata M 1971 *Mineral. J.* **6** 323
[22] Slack G A and MacNelly T F 1976 *J. Cryst. Growth* **34** 263
[23] Slack G A and MacNelly T F 1977 *J. Cryst. Growth* **42** 560
[24] Schwalter L J, Susterman Y, Wang R, Bhat I, Arunmozhi G and Slack G A 2000 *Appl. Phys. Lett.* **76** 985
[25] Schwalter L J, Rojo J C, Slack G A, Susterman Y, Wang R, Bhat I and Arunmozhi G 2000 *J. Cryst. Growth* **211** 78
[26] Rojo J C, Slack G A, Morgan K, Raghothamachar B, Dudley M and Schwalter L J 2000 *J. Cryst. Growth* **231** 317
[27] Bondokov R T, Mueller S G, Morgan K E, Slack G A, Schujman S, Wood M C, Smart J A and Schowalter L J 2008 *J. Cryst. Growth* **310** 4020
[28] Noveski V, Schlesser R, Freitas J A Jr, Mahajan S, Beaudoin S and Sitar Z 2003 *Mater. Res. Soc. Proc.* **798** Y2.8
[29] Noveski V, Schlesser R, Raghothamachar B, Dudley M, Mahajan S, Beaudoin S and Sitar Z 2005 *J. Cryst. Growth* **279** 13
[30] Epelbaum B M, Bickermann M and Winnacker 2005 *J. Cryst. Growth* **275** 479
[31] Zhuang D, Herro Z G, Schlesser R, Raghothamachar B, Dudley M and Sitar Z 2006 *J. Electr. Mater.* **35** 1513
[32] Nikolaev A, Nikina I, Zubrilov A, Mynbaeva M, Melnik Yu and Dmitriev V 2000 *MRS Internet J. Nitride Semicond.* **595** W6.5.1
[33] Melnik Yu *et al* 2003 *Phys. Status Solidi* a **200** 22
[34] Kumagai Y, Tajima J, Ishizuki M, Nagashima T, Murakami H, Takada K and Koukitu A 2008 *Appl. Phys. Express* **1** 045003
[35] Vodakov Yu A, Mokov E N, Roenkov A D, Boiko M E and Baranov P G 1998 *J. Cryst. Growth* **183** 10
[36] Kraler G, Zachara J, Podsiadlo S, Adamowicz L and Gebicki W 2000 *J. Cryst. Growth* **212** 39
[37] Dwiliński R, Doradziński R, Garczyński J, Sierzputowski L, Baranowski J M and Kamiñska M 1998 *Diamond Relat. Mater.* **7** 1348
[38] Yoshikawa A, Ohshima E, Fukuda T, Tsuji H and Oshima K 2004 *J. Cryst. Growth* **260** 67
[39] Aoki M, Yamane H, Shimada M, Sarayamana S and DiSalvo F J 2002 *J. Cryst. Growth* **242** 70
[40] Porowski S 1996 *J. Cryst. Growth* **166** 583
[41] Porowski S 1998 *J. Cryst. Growth* **189–190** 153
[42] Grzegory I and Porowski S 2000 *Thin Solid Films* **367** 281
[43] Grzegory I, Boćkowski M, Łucznik B, Krukowski S, Romanowski Z, Wróblewski M and Porowski S 2002 *J. Cryst. Growth* **246** 177
[44] Grzegory I and Porowski S 1999 *Gallium Nitride and Related Semiconductors* ed J H Edgar *et al* (*EMIS Datareviews Series* No 23) INSPEC p 359
[45] Boækowski M, Strak P, Grzegory I, Lucznik B and Porowski S 2008 *J. Cryst. Growth* **310** 3924
[46] Ballman A A, Dodd D M, Kuebler N A, Laudise R A, Wood D L and Rudd D W 1968 *Appl. Opt.* **7** 1387
[47] Wang B and Callahan M J 2006 *Cryst. Growth Des.* **6** 1227
[48] Ketchum D R and Kolis J W 2001 *J. Cryst. Growth* **222** 431
[49] Hashimoto T, Fujito K, Sharma R, Letts E R, Fini P T, Speck J S and Nakamura S 2006 *J. Cryst. Growth* **291** 100
[50] D'Evelyn M P, Hong H C, Park D-S, Lu H, Kaminsky E, Melkote R R, Perlin P, Leszczynski M, Porowski S and Molnar R J 2007 *J. Cryst. Growth* **300** 11
[51] Ehrentraut D, Kagamitani Y, Fukuda T, Orito F, Kawabata S, Katano K and Terada S 2008 *J. Cryst. Growth* **310** 3901
[52] Dwilinski R, Doradzinski R, Garczynski J, Sierzputowski L P, Puchalski A, Kanbara Y, Yagi K, Minakuchi H and Hayashi H 2008 *J. Cryst. Growth* **310** 3911

[53] Dwilinski R, Doradzinski R, Garczynski J, Sierzputowski L P, Puchalski A, Kanbara Y, Yagi K, Minakuchi H and Hayashi H 2009 *J. Cryst. Growth* **311** 3015
Dwilinski R, Doradzinski R, Garczynski J, Sierzputowski L P, Zajac M and Rudzinski M 2009 *J. Cryst. Growth* **311** 3058

[54] Kucharski R, Rudzinski M, Zajac M, Doradzinski R, Garczynski J, Sierzputowski L, Kudrawiec R, Serafinczuk J, Strupinski W and Dwilinski R 2009 *Appl. Phys. Lett.* **95** 131119

[55] Aoki M, Yamane H, Shimada M, Sarayama S, Iwata H and DiSalvo F J 2004 *J. Cryst. Growth* **266** 461

[56] Kawamura F, Morishita M, Tanpo M, Imade M, Yoshimura M, Kitaoka Y, Mori Y and Sasaki T 2008 *J. Cryst. Growth* **310** 3946

[57] Kawamura F, Tanpo M, Miyoshi N, Yoshimura M, Mori Y, Kitaoka Y and Sasaki T 2009 *J. Cryst. Growth* at press

[58] Feigelson B N, Frazier R M, Gowda M, Freitas J A Jr, Fatemi M, Mastro M A and Tischler J G 2008 *J. Cryst. Growth* **310** 3934

[59] Maruska H P and Tietjen J J 1969 *Appl. Phys. Lett.* **15** 327

[60] Kelly M K, Vaudo R P, Phanse V M, Gögens L, Ambacher O and Stutzmann M 1999 *Japan. J. Appl. Phys.* **38** L217

[61] Park S S, Park I-W and Choh S H 1999 *Japan. J. Appl. Phys.* **38** L217

[62] Paskova T, Darakchieva V, Paskov P P, Söderwall U and Monemar B 2002 *J. Cryst. Growth* **246** 207

[63] Yoshida T, Oshima Y, Eri T, Ikeda K, Yamamoto S, Watanabe K, Shibata M and Mishima T 2008 *J. Cryst. Growth* **310** 5

[64] Hanser D, Tutor M, Preble E A, Williams M, Xu X, Tsvetkov D and Liu L 2007 *J. Cryst. Growth* **305** 372

[65] Hanser D, Liu L, Preble E A, Udwary K, Paskova T and Evans K R 2008 *J. Cryst. Growth* **310** 3953

[66] Motoki K *et al* 2001 *Japan. J. Appl. Phys. Part 2* **40** L140

[67] Motoki K, Okahisa T, Hirota R, Nakahata S, Uematsu K and Matsumoto N 2007 *J. Cryst. Growth* **305** 377

[68] Lucznik B, Pastuszka B, Bockowski M, Kamler G, Litwin-Staszewska E and Porowski S 2005 *J. Cryst. Growth* **281** 38

[69] Grzegory I, Lucznik B, Bockowski M, Pastuszka B, Kamler G, Nowak G, Krysko M, Krukowski S and Porowski S 2006 *Phys. Status Solidi* a **243** 1654

[70] Leszczynski M, Suski T, Domagala J and Prystawko P 1999 *Gallium Nitride and Related Semiconductors* ed J H Edgar *et al* (*EMIS Datareviews Series* No. 23) INSPEC p 6

[71] Ponce F A, Bour D P, Young W T, Suanders M and Steeds J W 1999 *Appl. Phys. Lett.* **69** 337

[72] Liliental-Weber Z, Kisielowski C, Ruvimov S, Grzegory I, Bockowski M, Jun J and Porowski S 1996 *J. Electron. Mater.* **25** 1545

[73] Weyher J L, Muller S, Grzegory I and Porowski 1997 *J. Cryst. Growth* **182** 17

[74] Freitas J A Jr and Khan M A 1994 *Mater. Res. Soc.* **339** 547

[75] Bergman L, Dutta M and Nemanich R J 2000 *Raman Scattering in Materials Science* ed W H Weber and R Merlin (*Springer Series in Materials Science* vol 42) (Berlin: Springer) p 273

[76] Tischler J and Freitas J A Jr 2004 *Appl. Phys. Lett.* **85** 1943

[77] Freitas J A Jr, Braga G C B, Moore W J, Tischler J G, Culbertson J C, Fatemi M, Park S S, Lee S K and Park Y 2001 *J. Cryst. Growth* **231** 322

[78] Gil B, Briot O and Aulombard R L 1995 *Phys. Rev.* B **52** R17028

[79] Suzuki M, Uenoyama T and Yanase A 1995 *Phys. Rev.* B **52** 8132

[80] Shikanai A, Azuhata T, Sota T, Chichibu S, Kuramata A, Horino K and Nakamura S 1997 *J. Appl. Phys.* **81** 417

[81] Volm D, Oettinger K, Streibl T, Kovalev D, Ben-Chorin M, Diener J and Meyer B K 1996 *Phys. Rev.* B **53** 16543

[82] Chichibu S, Azuhata T, Sota T, Amano H and I Akasaki 1997 *Appl. Phys. Lett.* **70** 2085

[83] Kim K, Lambrecht W R, Segall B and van Schilfgaarde M 1997 *Phys. Rev.* B **56** 7363

[84] Chuang S L and Chang C S 1996 *Phys. Rev.* B **54** 2491

[85] Wei S-H and Zunger A 1996 *Appl. Phys. Lett.* **69** 2719

[86] Youngman R A and Harris J H 1990 *J. Am. Ceram. Soc.* **73** 3238

[87] Slack G A, Schowalter L J, Morelli D and Freitas Jr J A 2002 *J. Cryst. Growth* **246** 287

[88] Tuomisto F *et al* 2008 *J. Cryst. Growth* **310** 3998

[89] Senawiratne J, Strassburg M, Dietz N, Haboeck U, Hoffmann A, Noveski V, Dalmau R, Schlesser R and Sitar Z 2005 *Phys. Status Solidi* c **2** 2774

[90] Edgar J H, Du L, Nyakiti L and Chaudhuri J 2008 *J. Cryst. Growth* **310** 4002

[91] Neuburger M, Aleksov A, Schlesser R, Kohn E and Sitar Z 2007 *Electron. Lett.* **43** 592

[92] Silveira E, Freitas J A Jr, Slack G A and Schowalter L J 2003 *Phys. Status Solidi* c **0** 2618

[93] Silveira E, Freitas J A Jr, Glembocki O J, Slack G A and Schowalter L J 2005 *Phys. Rev.* B **71** 041201

[94] Moore W J, Freitas J A Jr, Holm R T, Kovalenkov O and Dmitriev V 2005 *Appl. Phys. Lett.* **86** 141912

[95] Silveira E, Freitas J A Jr, Schujman S B and Schowalter L J 2008 *J. Cryst. Growth* **310** 4007

[96] Perlin P, Camassel J, Knap W, Talercio T, Chervin J C, Suski T, Grzegory I and Porowski S 1995 *Appl. Phys. Lett.* **67** 2524

[97] Wetzel C, Suski T, Ager J W III, Weber E R, Haller E E, Fisher S, Meyer B, Molnar R and Perlin P 1997 *Phys. Rev. Lett.* **78** 3923

[98] Perlin P, Suski T, Leszczyński M and Teisseyre H 1997 *Optoelectronic Properties of Semiconductors and Superlattice* vol 2 *GaN and Related Materials* ed S J Pearton (London: Gordon and Breach) p 315

[99] Burnstein E 1954 *Phys. Rev.* **93** 632

[100] Moss T S 1954 *Proc. Phys. Soc.* B **67** 775

[101] Look D C and Sizelove J R 2001 *Appl. Phys. Lett.* **79** 1133

[102] Freitas J A Jr, Braga G C B, Moore W J, Lee S K, Lee K Y, Song I J, Molnar R J and Van Lierde P 2001 *Phys. Status Solidi* **188** 457

[103] Moore W J, Freitas J A Jr, Braga G C B, Molnar R J, Lee S K, Lee K Y and Song I J 2001 *Appl. Phys. Lett.* **79** 2570

[104] Moore W J, Freitas J A Jr, Lee S K, Park S S and Han J Y 2002 *Phys. Rev.* B **65** 081201R

[105] Freitas J A Jr, Moore W J, Shanabrook B V, Braga G C B, Lee S K, Park S S and Han J Y 2002 *Phys. Rev.* B **66** 233311

[106] Litwin-Staszewska E *et al* 1999 *Phys. Status Solidi* b **216** 567

[107] Freitas J A Jr, Gowda M, Tischler J G, Kim J-H, Liu L and Hanser D 2008 *J. Cryst. Growth* **310** 3968

[108] Kuznetsov N I, Nikolaev A E, Zubrilov A S, Melnik Yu V and Dmitriev V A 1999 *Appl. Phys. Lett.* **75** 3138

[109] Kneissl M, Yang Z, Teepe M, Knollenberg C, Schmidt O, Kiesel P, Johnson N M, Schujman S and Schowalter L J 2007 *J. Appl. Phys.* **101** 123103

[110] Silveira E, Freitas J A Jr, Kneissl M, Treat D W, Johnson N M, Slack G A and Schowalter L J 2004 *Appl. Phys. Lett.* **84** 3501

[111] Taniyasu Y, Kasu M and Makimoto T 2006 *Nature Lett.* **44** 325

[112] Mayer M, Pelzmann A, Kamp M, Ebling K J, Teisseyre H, Nowak G, Leszczyński M, Grzegory I, Porowski S and Karczewski G 1997 *Japan. J. Appl. Phys.* **36** L1634

[113] Kormitzer K, Ebner T, Tonke K, Sauer R, Kirchner C, Schwegler V, Kamp M, Leszczyński M, Grzegory I and Porowski S 1999 *Phys. Rev.* B **60** 1471

[114] Leszczyński M, Prystawko P and Porowski S 1999 *Gallium Nitride and Related Semiconductors* ed J H Edgar *et al* (*EMIS Datareviews Series* No 23) INSPEC p 391

[115] Freitas J A Jr, Moore W J, Shanabrook B V, Braga G C B, Lee S K, Park S S, Han J Y and Koleske D D 2002 *J. Cryst. Growth* **246** 307

[116] Murthy M, Freitas J A Jr, Kim J-H, Glaser E R and Storm D 2007 *J. Cryst. Growth* **305** 393

[117] Wickenden A E Koleske D D, Henry R L, Gorman R J, Twigg M E, Fatemi M, Freitas J A Jr and Moore W J 2000 *Electron. Mater.* **29** R114

[118] Glaser E R, Freitas J A Jr, Shanabrook B V, Koleske D D, Park S S and Lee K Y 2003 *Phys. Rev.* B **68** 195201

[119] Detchprohm T *et al* 2007 *J. Cryst. Growth* **298** 272

[120] Schmidt M C, Kim K-C, Sato H, Fellows N, Masui H, Nakamura S, DenBaars S P and Speck J S 2007 *J. Appl. Phys.* **46** L126

[121] Farrel R M *et al* 2007 *J. Appl. Phys.* **46** L761

[122] Kim K-C, Schmidt M C, Sato H, Wu F, Fellows N, Saito M, Fujito K, Speck J S, Nakamura S and DenBaars S P 2007 *Phys. Status Solidi (RRL)* **1** 125

[123] Liu J P *et al* 2008 *Appl. Phys. Lett.* **92** 011123

[124] Chakrabortty A, Keller S, Meier C, Haskell B A, Keller S, Waltereit P, DenBaars S P, Nakamura S, Speck J S and Mishra U K 2005 *Appl. Phys. Lett.* **86** 031901

[125] Enya Y *et al* 2009 *Appl. Phys. Express* **2** 082101

[126] Perlin P *et al* 2008 *J. Cryst. Growth* **310** 3979

[127] Storm D F *et al* 2007 *J. Cryst. Growth* **305** 34

[128] Zhou Y, Li M, Wang D, Ahyi C, Tin C-C, Williams J and Park M 2006 *Appl. Phys. Lett.* **88** 113509

[129] Ren Z *et al* 2007 *Appl. Phys. Lett.* **91** 051116

[130] Grandusky J R, Smart J A, Mendrick M C, Schwoltar L J, Chen K X and Schubert E F 2009 *J. Cryst. Growth* **311** 2864